Department of Physics and Astronomy
University of Heidelberg

Bachelor Thesis in Physics
submitted by

Judith Gafriller

born in Sterzing/ Vipiteno (Italy)

2019

^{222}Rn measurements in water for XENONnT

This Bachelor Thesis has been carried out by Judith Gafriller at the
Max-Planck-Institut für Kernphysik in Heidelberg
under the supervision of
Prof. Dr. Dr. h. c. Manfred Lindner

^{222}Rn measurements in water for XENONnT

XENON1T is currently the most sensitive experiment for direct dark matter search. In order to detect a dark matter particle scattering off a xenon nucleus, the background has to be diminished. Thence, the detector is surrounded by a water tank suppressing radiation and cosmic rays. For the upgrade XENONnT, the sensitivity will be further improved by enriching the water with gadolinium. It will allow to capture and detect neutrons created within the detector materials. In order to check whether the trigger rate of the neutron veto system is sufficiently low a radon background study is necessary. This work focuses on the development of a gas drying and purifying method which supports the well established technique of radon measurements with proportional counters. After introducing the radon measurement system at the MPIK, the performance of different gas drying techniques will be analysed. Finally the extended measurement procedure is presented and characterized.

^{222}Rn Messungen im Wasser für das XENONnT Experiment

XENON1T ist derzeit das empfindlichste Experiment für die direkte Suche nach dunkler Materie. Um die Wechselwirkung von dunkler Materie mit Xenonkernen zu detektieren, muss der Untergrund unterdrückt werden. Der Detektor ist daher von einem Wassertank umgeben, der Radioaktivität und Strahlung abschirmt. Für das Upgrade XENONnT wird die Empfindlichkeit weiter verbessert, indem das Wasser mit Gadolinium angereichert wird. Damit können Neutronen erfasst werden, die innerhalb der Detektormaterialien entstehen. Um zu überprüfen, ob die Triggerrate des Vetosystems ausreichend niedrig ist, ist eine Radon-Hintergrundstudie erforderlich. Diese Arbeit konzentriert sich auf die Entwicklung einer Gastrocknungs- und Reinigungsmethode, die die bewährte Methode der Radonmessung mit Proportionalzählern erweitert. Nach der Einführung des Radon-Messsystems am MPIK wird die Leistung verschiedener Gastrocknungstechniken analysiert. Zum Schluss wird das erweiterte Messverfahren vorgestellt.

Contents

1 Looking for the Invisible with XENON

The first estimations about the amount of dark, non-luminous matter in our universe started at the beginning of the 20th century [1]. Over the past decades, overwhelming observations of gravitational interactions between baryonic and dark matter have been made, but its nature stays a mystery up to the present. In various theories, it is assumed that still unknown, elementary particles account for dark matter. The identification of its nature could help to explain the evolution of our universe [2]. In order to gather evidence on the existence of such dark matter particles, many detectors have been built, which aim at measuring the interactions of these particles with baryonic matter.

1.1 Evidences for Dark Matter

The last century saw a number of astronomical and cosmological observations, many of which astounded physicists all over the world. At the beginning of the 1930s, J. H. Oort studied the vertical motion of stars in the Milky Way and estimated the dynamical density of matter in our galaxy. But the density calculated from the mass of visible stars did not correspond to the estimated dynamical density. Oort considered this discrepancy in mass as an indication for "invisible" [3] or "dark" matter in our galaxy.[4] At the same time, F. Zwicky calculated the velocities of individual galaxies in the Coma Cluster by observing their redshifts [5]. The results showed deviations from the virial velocities known beforehand from the mass of the cluster. Since the velocities of the galaxies were high, the visible mass was not enough for the cluster to be bound together. Zwicky came to the same conclusion as Oort; he introduced a non-luminous, dark matter component.[6] Furthermore, the standard model of cosmology (ΛCDM) permits to estimate the amount of dark matter in our universe. Ensuing from the cosmological principle (homogeneity and isotropy of the universe), one can establish the Friedmann-Lemaître-Robertson-Walker metric. Within the metric, $a(t)$ is a time-dependent scale factor and the constant $k \in \{0, \pm 1\}$ describes space curvature with $k = 0$ indicating a flat universe. By applying the foregoing assumptions, Einstein's field equation can be solved and results in the following Friedmann equations [7]:

$$\text{1st Friedmann eq.:} \quad H^2 = \left(\frac{\dot{a}}{a}\right)^2 = \frac{8\pi G}{3}\rho_{tot} - \frac{k}{a^2} \tag{1.1}$$

$$\text{2nd Friedmann eq.:} \quad \frac{\ddot{a}}{a} = -\frac{4\pi G}{3}\left(\rho_{tot} + \frac{3p}{c^2}\right) \tag{1.2}$$

Therein, G accounts for Newton's gravitational constant, H describes the Hubble parameter, p the pressure and $\rho_{tot} \approx \rho_{Matter} + \rho_\Lambda$ the total energy density of the universe. By introducing the density parameter Ω

$$\Omega = \frac{\rho_{tot}}{\rho_{crit}} \approx \Omega_{BM} + \Omega_{CDM} + \Omega_\Lambda \quad \text{with} \quad \rho_{crit} = \frac{3H^2}{8\pi G} \tag{1.3}$$

one can rewrite equation 1.1 in terms of Ω. Here, Ω_{BM} is the density parameter for the baryonic matter, Ω_{CDM} accounts for the cold dark matter and Ω_Λ for the vacuum energy. Whereas cold dark matter describes non-relativistic, non-baryonic matter. The different constituents of Ω can be determined by analysing the Cosmic Microwave Background (CMB). The CMB shows temperature fluctuations at a level of 10^{-5}K [8]. By assuming Gaussian temperature fluctuations, one can fit the ΛCDM-model to the power spectrum of the CMB and determine the best-fit criteria of the different density parameters [9]:

$$\Omega_{BM}h^2 = 0.02226 \pm 0.00023 \qquad \Omega_{CDM}h^2 = 0.1186 \pm 0.0020$$
$$\Omega_\Lambda = 0.692 \pm 0.012 \quad \text{with} \quad h = \frac{67.81 \pm 0.92}{100}$$

As shown above, the energy density of the universe consists of 69.2% dark energy, 25.8% dark matter and 4.8% baryonic matter. The dark energy term represents an unknown constant energy density which accounts for the accelerated expansion of the universe. Therefore, roughly 95 % of the universe is still unknown.

Today there exist many models, which predict different particles as dark matter candidates. The XENON experiment discussed in this work attempts to detect weakly interacting massive particles (WIMPs). The interested reader may refer to [10].

1.2 The XENON1T Experiment

The XENON1T experiment is located at the Laboratori Nazionali del Gran Sasso (LNGS) in Italy. Approximately 1400 m of solid rock shield the facilities and provide the low-background experiment with a protection from cosmic rays and atmospheric muons. As investigated in [11] and [12], the muon flux within the underground laboratory amounts to $(3.31 \pm 0.03) \cdot 10^{-4}\,\mathrm{muons/m^2/s}$ with an average energy of 270 GeV. Furthermore, the detector is submerged in a water tank which operates as an active Cherenkov muon veto that will be discussed in section 1.3. Currently, XEONON1T is the most sensitive detector for direct dark matter search for WIMP masses $> 6\ \mathrm{GeV}/c^2$. Figure 1 shows the latest results of the XENON1T detector. The most stringent upper limit of the WIMP-nucleon elastic scattering cross section was set at $\sigma_{SI} = 4.1 \times 10^{-47}\,\mathrm{cm}^2$ for a mass of 30 GeV/c^2 [13].

A detailed description of the working principle of the XENON1T detector can be found in [14],[15] and [16]. The detector is based on a dual-phase time projection

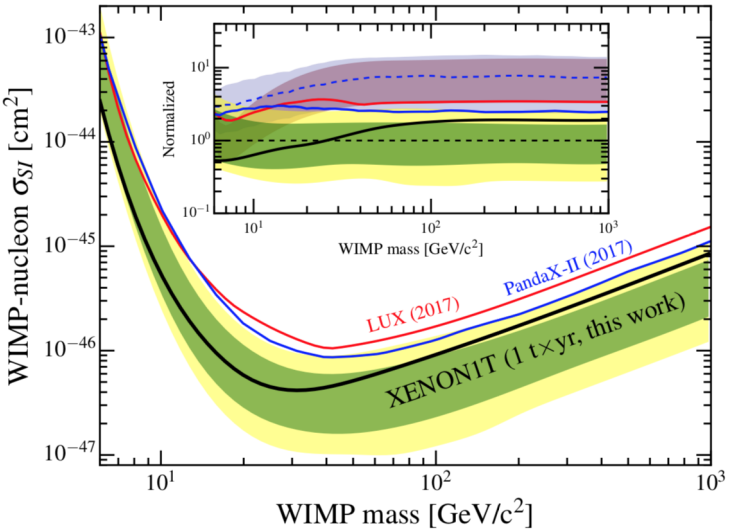

Figure 1: XENON1T results for the spin-independent dark matter search. The limit at a 90 % confidence level is given with the black line and the green and yellow parts represent the 1σ and 2σ sensitivity bands, respectively. The inserted plot displays the same results normalized to the median of the sensitivity band. The figure was taken from [13].

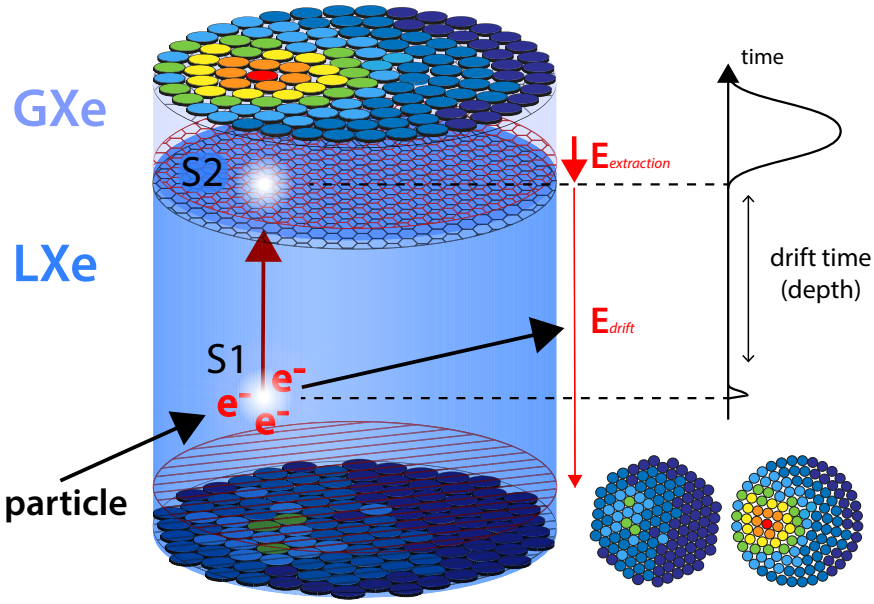

Figure 2: Working principle of a dual-phase Time Projection Chamber (TPC). The generation of primary and secondary scintillation signals is depicted including a schematic hit pattern at the PMT arrays.

chamber (TPC) filled with liquid xenon (LXe) as a target material and a gaseous xenon (GXe) volume above it.

The aim of the experiment is to detect WIMP scattering events inside the liquid xenon volume with ionisation and scintillation signals created in the scattering process. If a particle interacts with a nucleus in the liquid target, the transmitted energy causes excitation and ionisation of the surrounding xenon atoms, as shown in figure 2. While decaying to the ground state, excited xenon atoms emit primary scintillation photons with a wavelength of 178 nm which generates a light signal (S1) in the detector. In order to collect the electrons produced during the ionisation process, an electric field is applied across the liquid target. The electrons drift towards the liquid gas interface. A second electrical field generated at the liquid-gas interface extracts the electrons into the gas and accelerates them. With enough energy, the electrons excite and ionize the gaseous xenon. A secondary scintillation signal (S2) is generated which is proportional to the amount of extracted electrons. The photons of both processes are detected by photomultiplier

tube (PMTs) arrays employed at the top and the bottom of the TPC. The hit pattern of the S2 signal allows for a reconstruction of the horizontal (xy- coordinates) position of the interaction point. Due to a constant electron-drift velocity, the reconstruction of the vertical position of the interaction point is possible due to the time delay between S1 and S2 signals.

Background events that mimic WIMP signals should be avoided, especially because the WIMP rates are expected to be extremely low. Most of the background events are electronic recoil (ER) events produced by γ- or β-radiation interacting with electrons in the xenon atom shell. As WIMPs have no electrical charge, they will not see a repulsive coulomb barrier and will potentially interact with the xenon nucleus resulting in nuclear recoil (NR). The same accounts for neutrons or neutrinos that will also scatter off a nucleus and create a NR background event.

When it comes to an ER interaction, the probability of electrons recombining with the ionised xenon atoms is lower compared to the NR interaction, because a lower ionisation density is reached during an ER event. Therefore, the S2 signal of an ER event is augmented with respect to the S2 of a NR at the same energy which allows to differentiate between NR and ER events. This can be used to achieve a ER rejection rate of 99.75% at an acceptance for NR of 40 % [17]. NR background is more problematic because it is not possible to distinguish between WIMP interactions and NR background events. Hence it is important to suppress those background signals to the lowest possible limit.

1.3 The Water Veto System

1.3.1 The Cherenkov Water Tank for XENON1T

The XENON1T TPC is submerged in a cylindrical water tank with 10.2 m height and a diameter of 9.6 m [14], containing approximately 738 000 litres of highly purified water. The purpose of the tank is to shield the TPC from cosmic rays, muon-induced neutrons, γ-rays and external radioactive materials (e.g. rock). Figure 3 shows the passive shielding performance of the water tank. One can see that muon-induced neutrons are the only hazardous background remaining in the detector. Those are produced via muon spallation of nuclei or hadronic showers induced by muons. When a muon interacts with the detector components

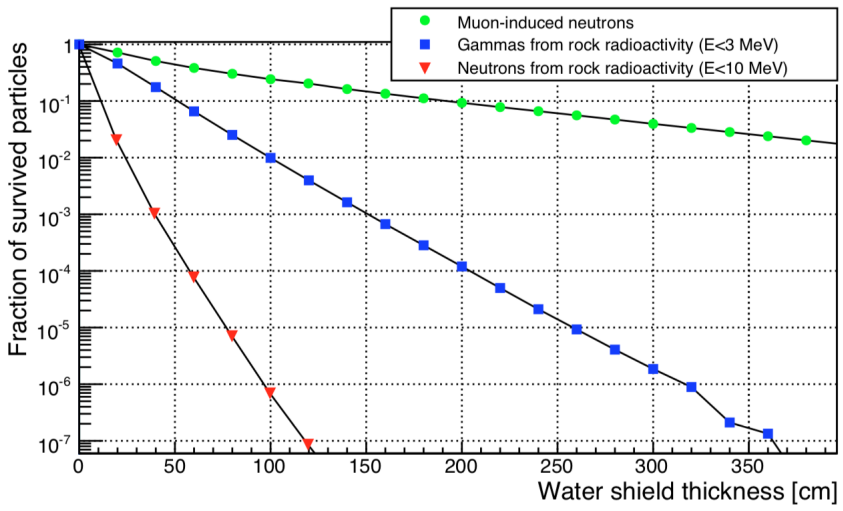

Figure 3: Simulation of remaining particles in the water tank as a function of water shield thickness. The green dots account for the muon-induced neutrons and the blue squares and red triangles represent background events induced by rock radioactivity. Figure taken from [18].

(eg. PMTs, stainless steel, PTFE shielding,...), neutrons can be produced that penetrate the LXe target, scatter off elastically from xenon nuclei and create a WIMP-like signal. In order to suppress the muon-induced background, the water tank operates as an active Cherenkov veto. Being equipped with 84 PMTs of a 20.3 cm diameter [14] it can detect the Cherenkov light that muons and their induced showers produce while passing the water. Thus, WIMP-like events can be matched with traversing muons and can be identified as NR background events. With this method, the muon-induced background rate can be reduced to $0.01(t \cdot y)^{-1}$ [16].

1.3.2 The Advanced Neutron Veto for XENONnT

Neutrons are not only induced by muons, but also by radioactive impurities in the detector materials [16]. Sources are spontaneous fission of isotopes from the thorium, the radium or the uranium series or when α-particles from these chains interact with nuclei in the detector materials and (α,n) reactions occur. Those radiogenic neutrons can mimic a WIMP event in case they scatter only once inside

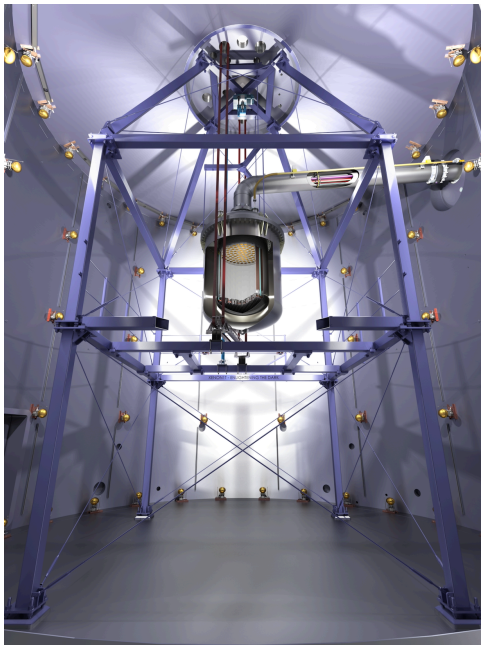

Figure 4: The XENON TPC is installed inside a water tank. PMTs are employed on the water tank walls for Cherenkov light detection. For the veto upgrade, another 120 PMTs will be installed on the lateral walls and the stainless steel support frame.

the active volume before leaving the detector towards the water tank. After the recoil, the neutrons can enter the water tank. In order to detect those neutrons, the water will be enriched with 0.2 % gadolinium as it has the highest thermal neutron capture cross-section of all stable nuclei [19]. To enrich the water with 0.2 % gadolinium, 0.48 % gadolinium-sulphate is needed which will result in 3.4 t gadolinium-sulphate-octahydrate ($Gd_2(SO_4)_3 \cdot 8\,H_2O$) once it is dissolved in water. In a gadolinium-enhanced neutron capture, the free neutron is absorbed by the gadolinium and both merge into a heavier Gd-isotope. The excited isotope decays into the ground state by emission of a γ-ray cascade which carries away the excitation energy. The γ-rays cause the ejection of electrons from their atoms via Compton scattering or convert into electron-positron pairs. The Cherenkov light of those electrons is detected and the initial WIMP-like signal can be identified as a NR event. The neutron tagging efficiency is estimated to be 86 % to 90 % by a Monte Carlo simulation.[20]

A schematic drawing of the XENON water tank can be seen in figure 4. For the XENONnT upgrade 120 additional PMTs will be installed at the walls of the tank and on the support frame of the TPC.

2 Radon emanation measurement facilities at MPIK

Radon is a crucial background source for the XENON experiment. In the following section the different aspects of radon induced events are summarized. Furthermore, the well established radon measurement technique with proportional counters is described. The measurement procedure was developed at MPIK in [21] and constantly improved [22]. As discussed later, these measurements provide a powerful tool to mitigate radon induced background.

2.1 Radon as a background source

Radon is a radioactive noble gas with the three naturally occurring isotopes: ^{219}Rn, ^{220}Rn and ^{222}Rn. They are components of the primordial decay chains of the long-lived isotopes ^{235}U, ^{232}Th and ^{238}U, respectively. ^{222}Rn is the radon isotope with the longest half-life time of 3.82 days. As can be seen in figure 5, ^{222}Rn is the decay product of ^{226}Ra.

Since traces of the long-lived parent nuclei of radon are present in every material, radon is constantly produced inside the detector by radioactive decay. Being chemically inert and due to its relatively long half-life time, ^{222}Rn can emanate from the detector materials and it reaches the LXe target. Especially the β-decaying daughters of the ^{222}Rn nuclide like ^{214}Pb are a crucial background source. The energy of the electron generated by the β-decay can vary over a continuous spectrum depending on the energy of the created antineutrino. If the electron has a very low energy it can induce events in the WIMP-search region.

Since ^{219}Rn and ^{220}Rn have comparatively short half-life times of 4 s and 56 s, respectively, they cannot reach the LXe target material in crucial amounts. Therefore, they are not significant as background sources.

Given these points, it is important to select detector materials according to their radon emanation rate in order to keep the ^{226}Ra and ^{222}Rn content to the lowest possible limit. Which is why it is so important to measure the radon emanation rate thoroughly.

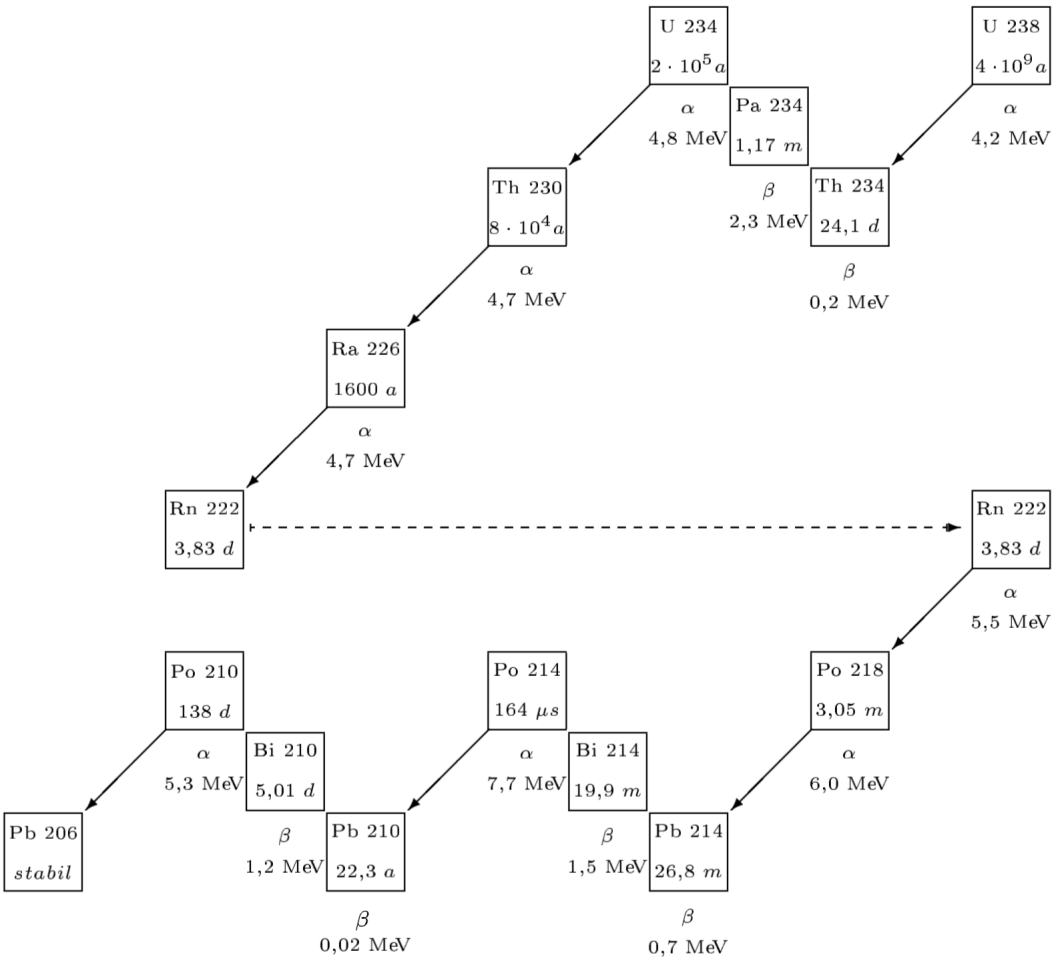

Figure 5: The ^{238}U decay chain.

2.2 Radon Emanation Measurements

2.2.1 Radon Extraction with AutoEma

The first step in the ^{222}Rn emanation measurement procedure is to put the sample into a vacuum tight container made from electro-polished stainless steel or glass. The enclosed air must be completely removed from the vessel, as its ^{222}Rn concentration can bias the measurement. Thus, the emanation chamber is evacuated and then filled with helium, which has been purified from radon by purging it through an active charcoal trap cooled with liquid nitrogen (LN_2). In case it is not possible to evacuate the chamber, it gets purged with purified helium for some

hours instead to remove the enclosed air. Radon will emanate from the sample with a constant rate. After some days the secular equilibrium has established. The radon is extracted by flushing the radon enriched helium from the vessel through an activated charcoal trap which is immersed in LN_2.

Due to its high polarisability, radon is efficiently bound to the surface of the activated carbon by means of van der Waals forces. This process is commonly known as adsorption. Moreover, cooling the active charcoal with liquid nitrogen will ensure that the radon will be adsorbed completely. Helium on the other hand will not be adsorbed by the cooled carbon due to its smaller mass. Therefore, the radon gets separated from the carrier gas which will be removed by a vacuum pump during the extraction process. Eventually, all radon is collected on the activated carbon and is ready to be filled into a radiation detector to determine the radon activity.

The extraction process described above is work- and time-consuming. As a consequence, it has been automatized during the last few years. A schematic drawing of the automatic extraction setup called "AutoEma" is shown in figure 6. AutoEma consists of two vacuum tight emanation chambers (E1 and E2) located in a clean room. An additional port (E3) is present to attach further sample containers. Two bakeable active charcoal traps are installed, one for carrier gas purification (A1) and the other one for radon collection (A2) during sample extraction. The cooling system consists of dewar vessels which can be filled with liquid nitrogen or liquid argon in which the traps will submerge. The filling level is monitored with weight sensors. The constant carrier gas flow and the stated pressure, which are mandatory for radon extraction are ensured by using two control valves (RV1 and RV2). All other valves are pneumatic below-seal valves. Before getting collected in the A2 trap, the sample is flushed through a hot, non-evaporating zirconium getter (A3). It removes organic impurities which might out-gas from the sample.

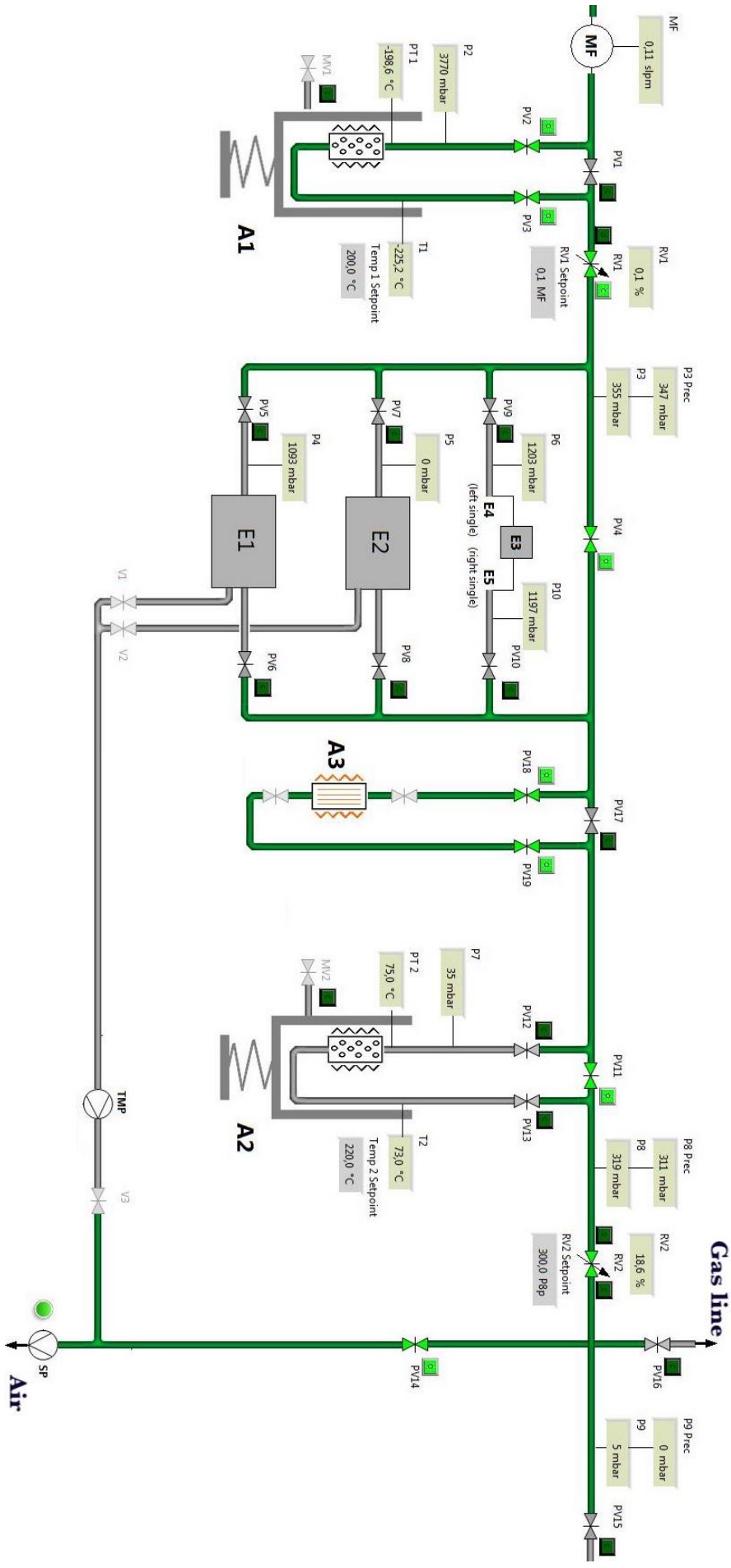

Figure 6: Picture of the AutoEma user interface.

AutoEma has two operational modes: manual and automatic. While operating AutoEma in the manual mode, all components e.g. valves, heating, getter etc. of a process can be controlled manually via a computer interface. For the automatic operation mode, a series of so-called extraction recipes are stored in a database. Recipes are predefined procedures with numerous different parameters chosen accordingly. The user can either chose one of the available recipes or create a new recipe for an individual procedure by defining parameters for the extraction steps. Parameters such as the gas flow, the pressure in the sample vessel or the temperature of the carbon trap are monitored and read out by an acquisition system. The extraction ends with the transfer of the collected radon from the carbon trap to the gas line used for proportional counter filling, which is described in the next section.

2.2.2 Activity Measurements with Proportional Counters

In order to measure the radon activity, proportional counters are employed which originally were established for the GALLEX/ GNO neutrino experiments [23]. The proportional counters are mostly made of quartz glass with a cylindrical cathode crafted of iron. The active volume enclosed by the cathode is approximately $1\,\mathrm{cm}^3$. A high voltage is applied between the cathode and the anode. In the middle of the sensitive volume, a thin anode wire at ground voltage is employed to collect electrons which are induced because of gas ionisation due to α-particles produced within the ^{222}Rn decay chain. Dominant background induced by γ-rays or muons can be efficiently rejected. The energy range of interest starts at 50 keV and the deposited energy of α-particles in the active volume is much higher than the energy muons can deposit on their short way through the counter. Within the energy range of interest for α-counting, proportional counters have a background rate of 0.4 to 3 counts per day [22]. This rate is expected to slowly increase over time, due to the long-lived radon daughter ^{210}Po, which will plate out on the counters' walls. Therefore, it is crucial to remove samples with a high activity as soon as possible, in order to guarantee the longevity of the counters.

In order to fill extracted radon into a proportional counter, the sample is transferred into the so-called gas line. In figure 7 a schematic drawing of the gas line

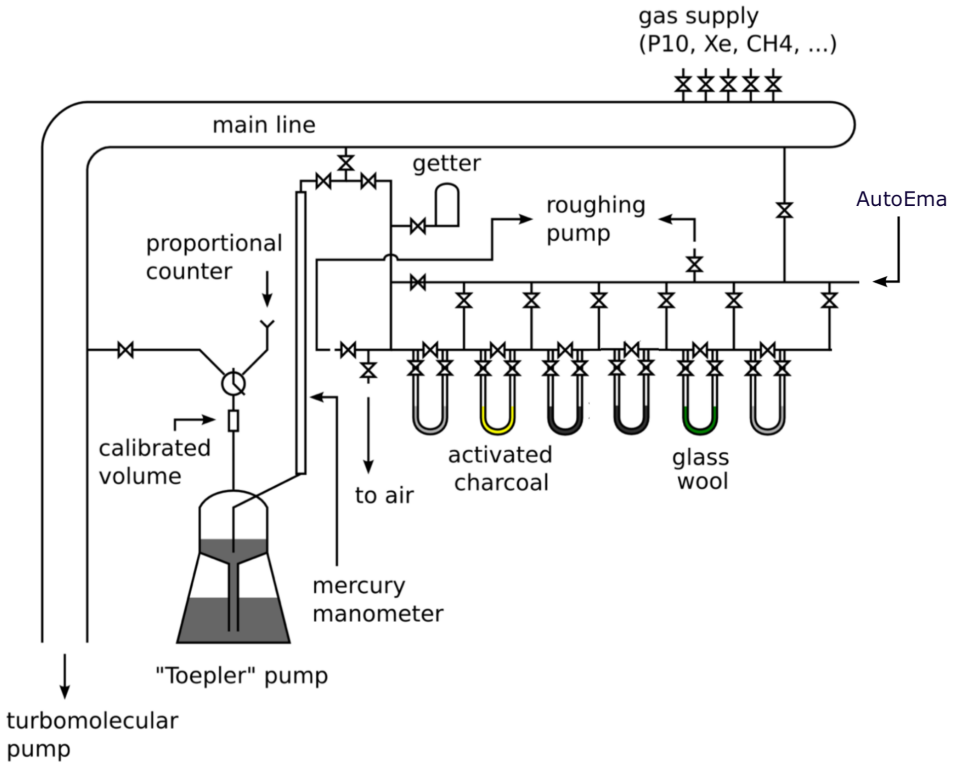

Figure 7: Schematic drawing of the counter filling gas line with the activated charcoal and H_2O traps.

at the MPIK is shown. It consists of different U-shaped traps filled with special adsorbers that can be operated at various temperatures. Remaining impurities can be removed from the sample by means of gas chromatography. Additionally, a hot getter installed at the end of the gas line. As a first step all traps need to be cleaned to make sure that all parts of the gas line are completely radon-free. For this purpose, the traps are heated to 100 °C to 200 °C depending on the adsorbent, while being pumped and flushed with purified, radon-free helium at the same time. Adsorbed radon will be desorbed and pumped away from the line.

After everything has been cleaned, the traps are cooled down. Not all traps shown in figure 6 are used for the here presented emanation measurements. The first employed trap is the so-called H_2O-trap which consists of densely packed glass wool and is submerged in a temperature bath of −20 °C. The following active charcoal trap is cooled with liquid nitrogen. The radon sample is purged

from the container through the H_2O-trap where especially water will freeze out. Afterwards, the sample passes the cooled activated carbon trap, where radon will be adsorbed and collected but helium pass through easily and will be removed by a roughing pump. After all radon has been transferred into the adsorbent trap of the gas line, the pumping is stopped and the trap gets heated in order to desorb the collected radon again. The desorbed gas is then exposed to a hot getter.

The last step is to transfer the collected radon into the clean (evacuated and baked) proportional counter. Before the ^{222}Rn-atoms are mixed with a counting gas consisting of 10 % argon and 90 % methane called P10. The amount of P10 is carefully measured with a manometer in order to make sure that the pressure in the counter will not exceed 1 atm after filling. The radon-P10 mixture is pushed into the counter using a Toepler pump which is operated with mercury. At the end, the filled counter is detached from the gas line and connected to the data acquisition and read-out system. The interested reader may refer to [24] and [22] for further details.

3 Radon emanation measurement procedure for liquid samples

For many low-background experiments, the radon concentration in liquids is crucial. This is also true for the XENONnT neutron veto introduced in section 1.3.2 where radon and its daughters might significantly contribute to the background-rate of the veto. The measurement procedure described in the last section however, can only be applied with solid emanation samples. The high humidity of the carrier gas causes different issues such as ice formation in the charcoal trap of AutoEma or the H_2O trap in the gas line(see section 2). Furthermore, the getter cannot get exposed to larger amounts of water. Thus, new techniques for gas drying need to be investigated and tested for their applicability in the radon emanation measurements.

In this chapter two gas drying techniques are investigated for their applicability in radon emanation measurements of liquid samples. In the final section a measurement of a radon standard mixed in water is performed.

3.1 Measurement of the gas humidity during sample extraction

As a first step towards a new procedure, the humidity of the carrier gas was measured as it is expected during the standard emanation measurement. A schematic drawing of the used setup is depicted in figure 8. The helium flow was monitored with a mass flow controller (MFC) at the beginning of the setup. A glass vessel filled with 100 ml to 500 ml water represents the liquid emanation sample.The helium carrier gas purges through the water recipient and gets humidified. The humid helium is then flushed through a test pipe which can be exchanged to different lengths. At the end of the test pipe a capacitive hygrometer measures the relative humidity [%RH] of the gas flow. Relative humidity describes the ratio of the water vapour present in the measured gas to the amount of water vapour at saturation. It is highly dependent on the gas temperature, however the changes of atmospheric pressure and room temperature in the laboratory are negligible.

The humidity measurements only have a qualitative character with the purpose

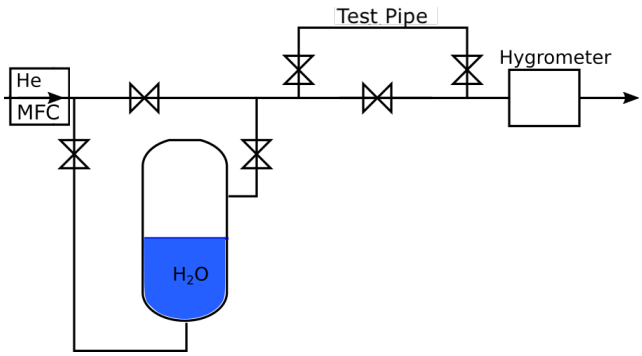

Figure 8: Experimental setup with a glass vessel filled with water, hygrometer and exchangeable test pipes.

to compare different settings. According to the manufacturer the hygrometer has a systematic error of 3 % RH. Since this error applies to all measurements the same way only the central values are shown for a relative comparison among the different measurements.

Various measurements with different helium flows, test pipe lengths and water amounts (i.e. filling level inside the vessel) have been performed. Figures 9 to 12 show the results of these measurements.

Dependence on the Helium Flow The humidity of the carrier gas was studied with different helium flows of 0.26, 0.60 and 1.15 slpm. For each measurement, the relative humidity was measured over time as shown in figure 9. The humidity is observe to rise fast within the first minutes until it slowly saturates. The

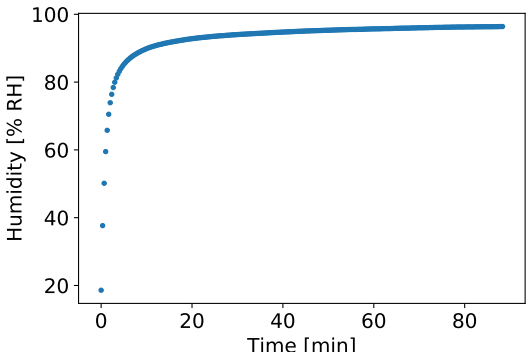

Figure 9: Time evolution of the relative humidity for a helium flow of 0.26 slpm.

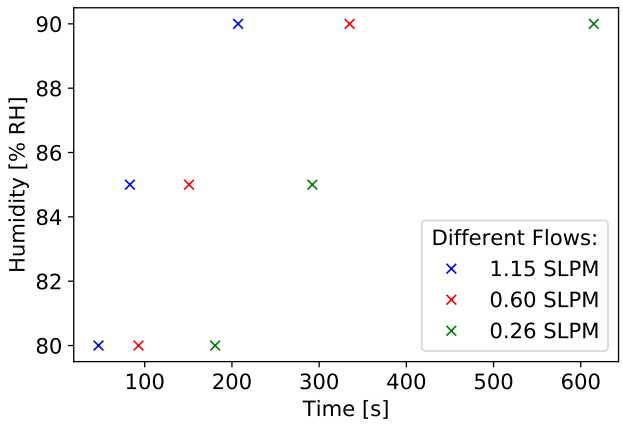

Figure 10: Interpolated results of the measurements with varying helium flows.

fast increase is explained by condensation of vapour which suppresses the relative humidity in the first minutes. Due to water vapour losses in the piping and an offset of the hygrometer 100 % RH was never reached.

The time evolution for each helium flow was interpolated at 80 %, 85 % and 90 % relative humidity which resulted in figure 10. For comparison, figure 10 shows that it takes less time to reach the maximal humidity with a higher flow. A higher flux means a bigger gaseous volume per second, therefore a bigger amount of water vapour can be carried.

Different Tubing Lengths Three hoses of different lengths have been installed in turn as the test pipe (see figure 8). Measurements have been performed at two different fluxes: 0.26 slpm and 1.36 slpm. The three different tubes in use had the lengths of 8.30 m, 4.10 m and 2.05 m, respectively. Again, the evolution of the relative humidity has been monitored and then interpolated results at 80 %, 85 % and 90 % are shown in figure 11. The longer the piping, the longer it takes to reach 100 % RH.The results obtained for 2.05 m and 4.10 m. This could be due to the fact that the piping system was not completely dry at the beginning of the measurements. The figure underlines the above stated argument that the time evolution of the humidity is dependent on the flow. One can see that it takes nearly 7 minutes more to reach 90 % RH for the smaller flow.

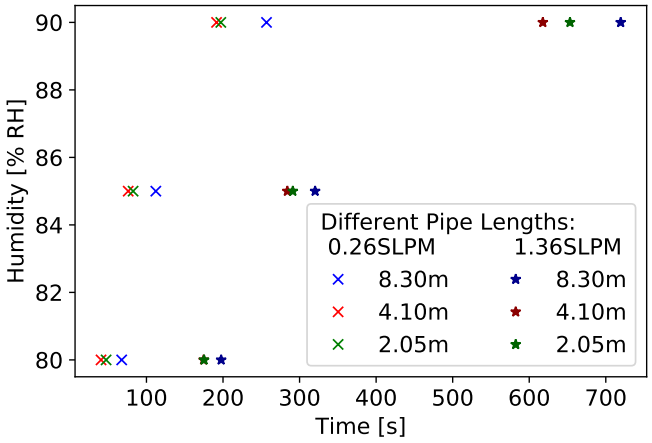

Figure 11: Interpolated results of the measurements with 1.36 and 0.26 slpm helium.

Different Water Volumes During the first measurement, the vessel was filled with a water volume of approximately 100 ml. Afterwards the water content was augmented to 500 ml. Measurements were conducted with 0.26 and 1.36 slpm helium for both water volumes. The results of the measurements are presented and summarized in figure 12. The plot shows that the filling level in the water recipient doesn't have any impact on the timescale until the helium is saturated with water vapour at the hygrometer.

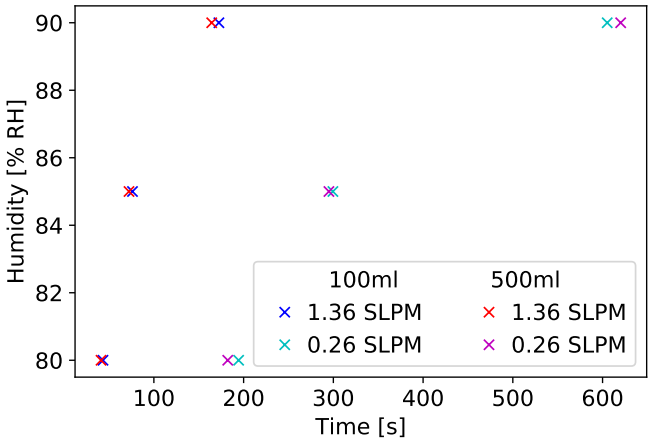

Figure 12: Interpolated results of the measurements with different filling levels.

3.2 Gas Drying Techniques

The expected humidity of the carrier gas is too high for the standard emanation measurement procedure. Therefore, a drying technique needs to be developed which can be integrated in the measurement procedure. The drying technique should remove all water vapour. Additionally, no radon should get lost during the drying process. In this section, different techniques are discussed and tested.

3.2.1 Nafion DryStick

The DryStick is a coaxial tubing system produced by PermaPure LLC with the purpose to dry gaseous streams. It consists of a inner tube enclosed by another pipe (see figure 13). The inner tube of the DryStick is made of Nafion, a copolymer of tetrafluoroethylene and perfluoro-3,6-dioxa-4-methyl-7-octene-sulfonic acid [1]. The sulfonic acid groups in the polymer absorb the water molecules (13 per group) from the sample gas. Due to the high affinity of sulfonic acid to water, the water molecules absorbed on the surface of the inner tube pass on to acid groups situated deeper within the material until they reach the outer surface. In this section

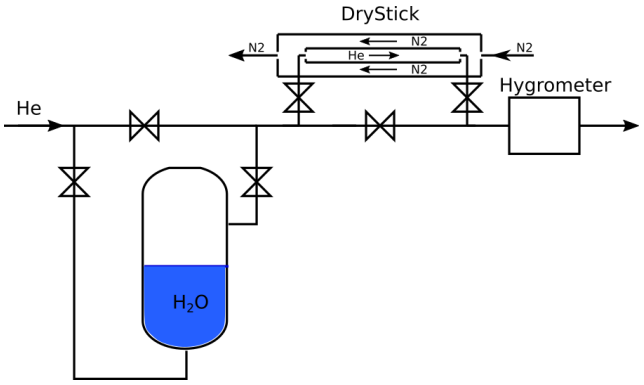

Figure 13: Experimental setup with the DryStick mounted at the piping system.

the drying efficiency of the DryStick is analysed as a function of different flows employing the setup sketched in figure 13. The maximal allowed flow through the DryStick is 4 slpm. Helium is used as sample gas and streams through the water in the glass vessel where it gets humidified. The helium flow is monitored with a mass flow controller (MFC) at the beginning of the setup. There they evaporate

[1] http://www.permapure.com/resources/all-about-nafion-and-faq/

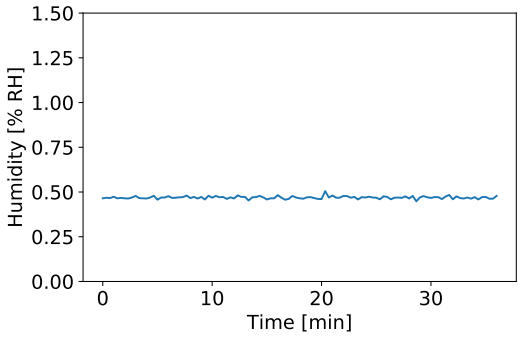

(a) Time evolution of the relative humidity while employing the DryStick at a sample flow of 0.26 slpm.

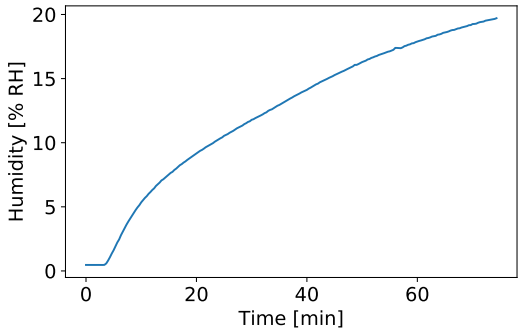

(b) Time evolution of the relative humidity while employing the DryStick at a sample flow of 1.36 slpm.

Figure 14: Comparison of the results with the same purge gas flow of 1 slpm but different sample gas flows.

into the purge gas which flows through the outer tube of the DryStick. For better performance, the purge gas should flow counter to the sample gas flow in the inner tube. The DryStick used in this work was 2.8 m long (serial number: MD-110-96FS-4). Afterwards, the helium flows through the inner part of the DryStick and gets dehumidified. N_2 is used as a purge gas and streams through the outer tube in the opposite direction of the helium.

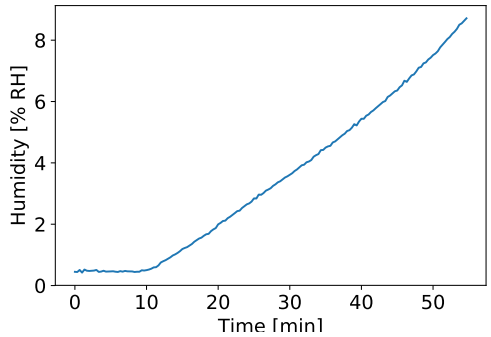

(a) Time evolution of the relative humidity while employing the DryStick at a purge flow of 0.2 slpm nitrogen.

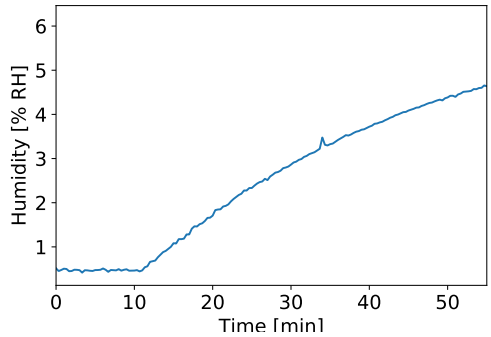

(b) Time evolution of the relative humidity while employing the DryStick at a purge flow of 1 slpm.

Figure 15: Comparison of the results with the same sample gas flux of 0.67 slpm but different purge gas flows.

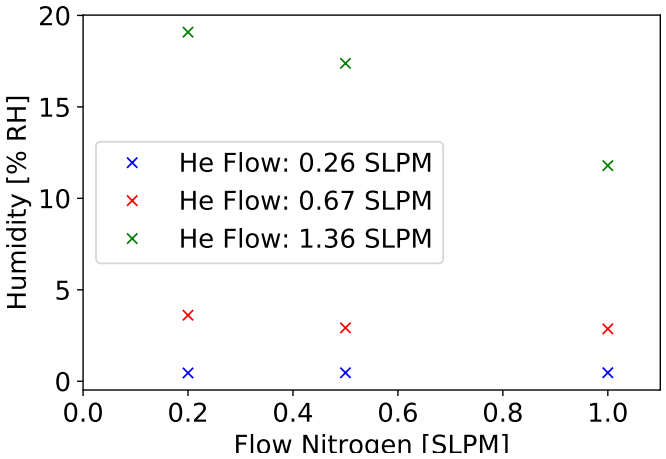

Figure 16: Summary of all measurements with interpolation at 30 min.

Different flow combinations of He and N_2 were tested. The outcome is shown in figure 14 and 15. The best performing combination is a small sample gas flow and a comparatively high purge gas flow. This relation can be seen in figures 14 and 15. Figure 14 shows a comparison of the impact of the sample gas flow while the purge gas flow was for both measurements the same.

At the beginning of all runs we observe, that the DryStick is able to remove all water vapour from the sample gas. Depending on the flow settings, after some time the relative humidity starts to rise. At some point, the amount of water molecules is too high and not all of them will find a free spot to bind with the sulfonic acid groups. This leads to an increase of humidity until the binding velocity of the molecules and the streaming velocity are in equilibrium. Figure 15 shows a comparison of the impact of the N_2 purge flow. This time the sample gas flow stays the same for figure 15b and 15a. One can see that for a higher purge gas flow the humidity equilibrium is at a lower point that with a lower purge gas flow. In figure 15b the humidity is on the edge of reaching the constant plateau where absorbing and flow rate are in balance. Whereas in figure 15a no plateau is visible yet. Figure 16 is a summary of all measurements. An interpolation after 30 minutes of all measured flux combinations was done. It underlines and reassures the discussion above.

Out-gassing measurements During the measurements using the Drystick a high out-gassing was observed. In order to identify its composition a residual gas analysis (RGA) measurement was performed. In a first background measurement helium was flushed through the setup shown in figure 13 but bypassing the water recipient and the DryStick. The helium was then passed trough an adsorbent trap at LN_2 temperature to collect the out-gassing impurities. This run is later referred to as the blank measurement. This same procedure was repeated while the helium passed through the DryStick.

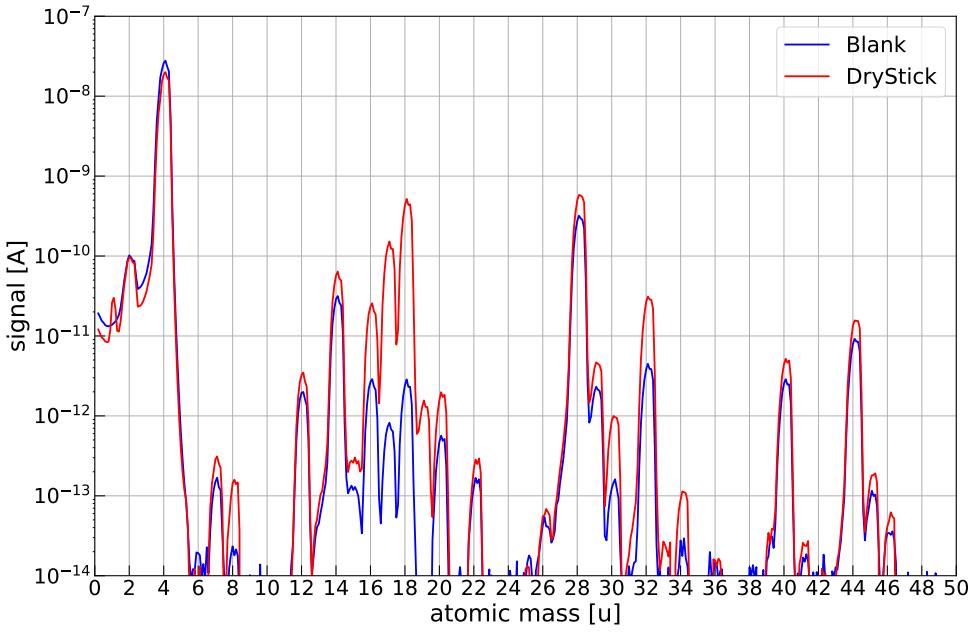

Figure 17: Out-gassing spectrum of the DryStick compared to the blank measurement.

In figure 17 a comparison of the blank and the DryStick measurement is shown. Compared to the blank, the DryStick shows high out-gassing of nitrogen, oxygen and water. In table 1 the highest peaks are listed with their assigned molecules. The highest peak is due to helium because it was used as carrier gas. No peaks higher than 50 u appeared. Both measurements (background and with DryStick) were analysed four times but all analyses showed similar results.

Atomic Mass [u]	Molecules	Chemical Symbol
4	Helium	He
12	Carbon	C
14	Methylene	CH_2
16	Oxygen	O
17	Hydroxyl group	OH
18	Water	H_2O
19	Fluorine	F
20	Hydrogen fluoride	FH
28	Nitrogen	N_2
30	Methanal	COH_2
32	Oxygen	O_2
44	Carbon dioxide	CO_2

Table 1: Highest peaks with corresponding molecules.

3.2.2 Cooling Trap with Glass and Copper Wool

During this work also the drying efficiency of glass and copper wool was studied. The experimental setup is shown in figure 18 on the next page. Helium purges through the water vessel and passes hereafter a cooling trap filled with copper or glass wool which is acting as a siccative. The cooling trap is immersed in a cooled ethanol bath, which allows the water vapour in the helium to freeze-out on the cold wool. Several measurements with different helium fluxes and temperature settings were performed. Figure 19 on the next page shows the results of all measurements. As expected, the drying efficiency is highly dependent on the temperature of the cooling trap. Furthermore, the measurements suggest that the helium flow does not have any major influence on the humidity in the tested flow range. Additionally, glass and copper wool show the same drying efficiency.

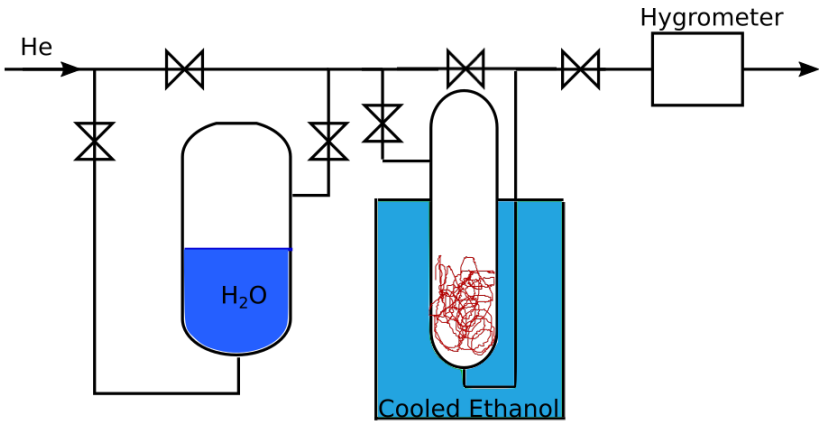

Figure 18: Experimental setup with cooling trap in a temperature bath acting as a siccative.

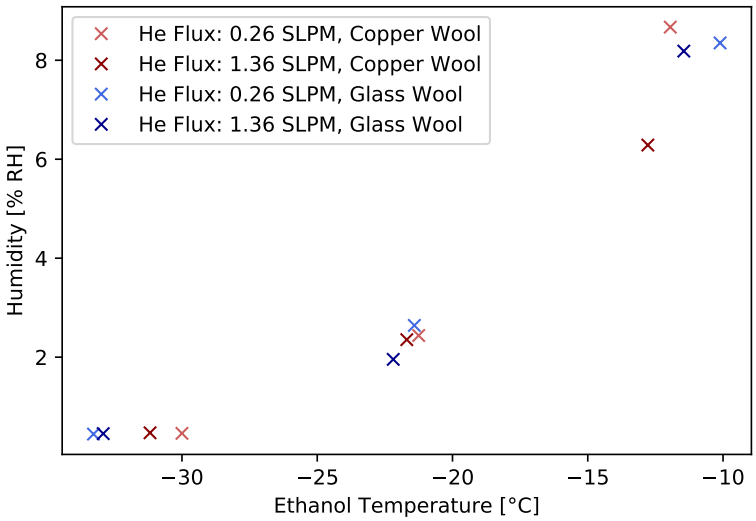

Figure 19: Results of all taken measurements interpolated at 30 minutes.

3.2.3 Radon Loss during the Gas Drying Process

Before being used, the above described drying methods were investigated in potential radon losses or additional radon emanation during the drying process. A high emanation rate of the DryStick or the copper wool would significantly contribute to the measured radon activity and thus bias the measurement. On the other hand it is possible that radon from the emanation sample gets lost during gas drying.

In order to determine the emanation rate of the DryStick it's inner pipe was filled with radon clean helium. After several days, the helium was extracted from the DryStick and the sample was measured. The DryStick showed an emanation rate of $(0.283 \pm 0.038)\,\mathrm{mBq}$. The background rate of the copper wool was measured in [25] showed a rate of $(2.5 \pm 0.1)\,\mathrm{mBq\,kg^{-1}}$. It should be noted that the emanation from the DryStick or the copper wool contributes only during the drying process, that is for a few hours at maximum. Thus, in many cases their effect on the total result is negligible but needs to be considered for very low activities.

In order to quantify potential losses of the radon sample due to the DryStick some measurements using a radon standard have been performed. The source consists of a polyester foil with an attached filter paper snippet. The radioactive solution, which emanates $^{222}\mathrm{Rn}$, was applied to the paper shred and is covered with additional polyester foil. The compound is mounted onto a holder which is contained in a glass vessel. The experimental setup for these radon loss tests is the same as depicted in figure 13. The radioactive source was placed before the water recipient filled with 500 ml water. First, the carrier gas was flushed only through the vial and the DryStick. Afterwards, it was guided through the vial, purged through the water and was dehumidified by the DryStick. The radon sample was then collected on the active charcoal trap of AutoEma and filled into a proportional counter for data analysis.

The procedure was conducted again with the copper wool trap mounted instead of the DryStick. The cooling trap was filled with 500 g of copper wool and operated at a temperature of $-30\,^{\circ}\mathrm{C}$. The results of the measurements are shown in table 2. It shows that neither the DryStick nor the copper wool trap lose radon during the drying process. However, the helium purging only lasted for 30 minutes. In order to strip radon completely from the water, the purging time needs to be increased

Date	Activity [mBq]	Drying Technique	water
18/05/2018	57.94 ± 4.34	DryStick	no water
30/05/2018	59.50 ± 3.55	DryStick	no water
21/06/2018	63.28 ± 3.48	DryStick	with water
09/10/2018	61.65 ± 2.85	Copper wool trap	with water
19/10/2018	62.53 ± 4.71	Copper wool trap	with water

Table 2: Summary of first radon loss tests with the DryStick and the copper wool. The radon standard was used as a sample.

with bigger water volumes as we will discuss in the next chapter.

In order to test the radon loss of the DryStick with bigger volumes, a radon source with known activity was placed in a large emanation vessel. 45 viton sealing o-rings served as a source. The radon was extracted from the vessel by purging it with clean helium for 150 minutes. First the source was measured without the DryStick, afterwards the DryStick was added in the procedure.The results of the measurements are summarized in table 3. The results show that no radon got lost during the procedure with the DryStick and they are compatible with past activity measurements.

Date	Activity [mBq]	
24/04/2013	33.29 ± 3.07	past result
09/11/2018	30.24 ± 1.56	no DryStick
13/11/2018	33.63 ± 1.80	no DryStick
16/11/2018	34.22 ± 1.59	with DryStick
21/11/2018	31.01 ± 1.63	with DryStick

Table 3: DryStick extraction efficiency measurements without water.

3.3 Emanation measurements of liquid samples

In the previous section, the drying efficiency and the radon loss potential of different methods has been studied. Now those techniques need to be integrated and tested in the standard emanation measurement procedure. In this section a procedure is developed for processing liquid samples of a large volume.

3.3.1 Radon extraction from water

Radon is present in water because of dissolved ^{226}Ra. In order to measure radon in water, the radon has to be isolated first. As the solubility of radon in water is poor, stripping is an efficient way to extract the radon from water [21] [22]. If a clean, radon-free gas flows through the water, the soluble radon transfers into the gaseous phase and is flushed out with the carrier gas. First, the theoretical aspects are discussed. A detailed discussion of the following theory can be found in [21] and [22].

For the following calculations, let N be an amount of moles of the substance marked in the subscript. For a small radon concentration, the molar fraction X^g of the carrier gas helium is given in the following equation. The superscript g indicates the molar fraction of radon in the gaseous phase whereas the superscript l is an indication for the liquid phase.

$$X^g = \frac{N^g_{Rn}}{N^g_{tot}} = \frac{N^g_{Rn}}{N^g_{Rn} + N^g_{He}} \approx \frac{N^g_{Rn}}{N^g_{He}} \quad \text{it follows:} \quad N^g_{Rn} = \frac{V_{He} P_{He}}{RT} X^g \tag{3.1}$$

with V_{He} as the volume, P_{He} as pressure and T as the temperature of the carrier gas and R describes the molar gas constant.

If a known volume dV_{He} of carrier gas flushes through a vessel filled with water, the amount of moles of radon stripped out is given as:

$$d(N^g_{Rn}) = dV_{He} \cdot \frac{P_{He}(X^g_{out} - X^g_{in})}{RT} \tag{3.2}$$

X^g_{in} describes the molar fraction of radon in the carrier gas entering the water vessel and X^g_{out} is the molar radon fraction leaving the water vessel. During a time dt and with a constant gas flow F_{He} a helium volume $dV_{He} = F_{He} \cdot dt$ was flushed through the water vessel. Under the assumption that the carrier gas is completely radon-free ($X^g_{in} = 0$) when it enters the vessel, the molar faction of radon carried away can be rewritten as:

$$\frac{d(N^g_{Rn})}{dt} = \frac{F_{He} P_{He} X^g_{out}}{RT} \tag{3.3}$$

Further, the following equation describes the amount of radon moles leaving the

water volume via the carrier gas:

$$\frac{d(N_{Rn}^l)}{dt} \overset{(3.1)}{=} \frac{d}{dt}(X_{out}^l \cdot N_{tot}^l) \approx N_{H_2O}^l \cdot \frac{dX_{out}^l}{dt} \tag{3.4}$$

$N_{H_2O}^l$ describes the number of moles of water and X_{out}^f stands for the molar fraction of radon that left the water volume. In equation 3.4 the assumption was made that the amount of water moles is much higher than the amount of radon moles.

As the amount of radon moles being stripped from the water volume is the same as the amount of radon leaving the vessel with the carrier gas, it is possible to state the following:

$$\frac{d(N_{Rn}^l)}{dt} = -\frac{d(N_{Rn}^g)}{dt} \qquad \text{and therefore:} \tag{3.5}$$

$$N_{H_2O}^l \cdot \frac{dX_{out}^l}{dt} = -\frac{F_{He} P_{He} X_{out}^g}{RT} \tag{3.6}$$

Henry's law defines a relation between the molar fraction of a gas dissolved in a liquid volume and its partial pressure in the gas phase. It is applicable if the concentration of the dissolved gas is small and everything is in thermal equilibrium. Applied to the scenario described in this section, *Henry's law* reads as follows:

$$X_{out}^g \cdot P_{He} = X_{out}^l \cdot H \tag{3.7}$$

H stands for Henry's constant. By applying *Henry's law* to equation 3.6 it results in the following differential equation:

$$\frac{dX_{out}^l}{X_{out}^l} = -\frac{F_{He} H}{RT N_{H_2O}^l} \cdot dt \tag{3.8}$$

By solving the differential equation above for $X_{out}^l(t = 0) = X_{in}^l$ we obtain:

$$X_{out}^l(t) = X_{in}^l \cdot \exp\left(-\frac{F_{He} H}{RT N_{H_2O}^l} \cdot t\right) \tag{3.9}$$

Equation 3.9 shows that most of the radon can be extracted by increasing the time of helium flowing through water. But, at the end of the procedure, the carrier

gas is saturated with water vapour which is why a gas drying method has to be developed.

3.3.2 Measurement of a radon enriched water sample

In this final section the investigated drying methods are used in an actual emanation measurement. 25 l of deionized water, enriched with radon from a standard are used as a sample.

In preparation of the measurement the DI-water was produced and filled into a 80 l stainless steel vessel. After closing the vessel it was flushed with clean helium in order to remove air and radon origin from air dissolved in the water. Thereby, the helium is flushed trough a sparger, located at the bottom of the vessel inside the water sample. The sparger should guarantee that the helium flows homogeneously through the water and flushes out the dissolved radon in the liquid. This process was done for about 150 min at a helium flow of 2 slpm.

In this measurement the water was enriched with a known amount of radon from the radon standard described in section 3.2.3. For the radon enrichment, the standard was connected at the inlet of the stainless steel vessel. Then, the radon was flushed from the standard with a constant helium flow directly into the vessel though the sparger. Since it might take some time until the radon dissolves homogeneously in the liquid a waiting time of 2-3 days followed the enrichment procedure. In order to extract the radon from the water, the vessel was flushed with 2 slpm of purified helium for 150 min.

As discussed in section 3.2.1, the DryStick alone cannot remove all water from the carrier gas-flow over the long time scales needed for the extraction process. As a consequence the copper wool cooling trap was employed after the DryStick. The trap was kept at a temperature of $-30\,^{\circ}\mathrm{C}$ as it turned out to be the best performing setting, see section 3.2.2.

After the extraction procedure, the frozen water in the copper wool was tested for radon. The copper wool was baked at $100\,^{\circ}\mathrm{C}$ in order to vaporize the ice in the trap. The sample was flushed through the DryStick which removed the remaining water vapour. Afterwards the sample was further processed with AutoEma.

Table 4 summarizes the results of the water extraction and the copper wool

Date	Activity [mBq]	Radon in trap [mBq]
12/12/2018	51.59 ± 2.60	n.a.
09/01/2019	51.83 ± 2.37	2.21 ± 0.16
15/01/2019	47.76 ± 2.49	1.99 ± 0.21
21/01/2019	46.53 ± 2.37	3.98 ± 0.31
25/01/2019	38.69 ± 2.79	n.a.

Table 4: Summary of the radon extraction efficiency tests with DryStick and copper wool trap employed. The radon enriched water was used as a sample.

extraction measurements. It shows that the measurements of the water extraction agree when taking the radon lost in the copper into consideration. By comparing the results in table 4 to table 2 one can see that the measurements are not consistent. It could be that not all radon was extracted from the water after all. In order to remove all radon, the extraction time could be extended. An increase of the helium flow could also improve the extraction efficiency.

The measurement conducted on the 25/01/2019 is not consistent with the previous measurements. Therefore, the radon source was measured with a standard procedure without any water or drying process on the 28/01/2019 and again on the 01/02/2019. The results are (40.83 ± 3.01) mBq and (42.12 ± 3.22) mBq, respectively. These results show a still unknown, systematic error of the radon standard used in the measurement procedures as previous measurements showed an activity of approximately 60 mBq (see section 3.2.3).

Further, the measurements of the cooling trap are not consistent, as table 4 shows. This could be due to the cooling system in use. It consisted of a cooling coil and a temperature sensor immersed in the cooling liquid. The coil regulated the temperature of the liquid according to the temperature sensor. The mean temperature of the liquid was dependent on the position of the sensor. This results in different temperatures of the cooling trap for different measurements. Therefore, the discrepancies of the measurements could be explained by the fact that more radon froze on the copper wool when the trap was colder.

4 Summary and conclusion

This work aimed to extend and optimize the well established radon measurement procedure with proportional counters at MPIK, as so far it was not applicable for liquid samples. As a first step a carrier gas is flushed through the sample to extract the radon. The main problem is the water vapour in the carrier gas: As the radon collection trap is employed at LN_2 temperatures, water would freeze on the activated charcoal and hinder radon collection. Therefore a gas drying method needs to be developed and integrated in the procedure.

During the measurement a carrier gas is used to extract radon from the sample vessel. In the first part of this thesis, the humidity of the carrier gas was studied. Measurements with several different parameters showed that the time evolution of the humidity depends on the helium flow and on the piping length. As water vapour will condense in the piping, the humidity will not reach its maximum instantaneously. A higher gas flow entails that the maximal humidity is reached faster. The same accounts for shorter piping lengths.

For the new procedure for liquid samples, the gas drying efficiency of two different methods was tested. The DryStick performed well with small helium flows, but at higher flows, after some time humidity started rising until it reaches a plateau. It was found that the DryStick is capable of removing most of the water vapour. The performance of the cooling trap filled with copper or glass wool is not dependent on the gas flow, but on the temperature it is operated at. Measurements showed that the performance is better the lower the operating temperatures are set. Later on, both drying methods were tested for their radon loss potential. Measurements with different radon sources showed that no radon was lost when applying the drying techniques.

In the last part of the thesis, the drying techniques were integrated in the extraction procedure. As the DryStick was not able to remove all water vapour, additionally to the DryStick the cooling trap was employed. Despite previous results, during these measurements it was found that radon does freeze out on the copper wool. It's activity can be determined in a separate measurement when warming up the cooling trap after the actual radon extraction from the liquid sample. The radon freeze out at the cooling trap probably depends on the operating

temperature of the cooling trap. Further measurements with different operating temperatures need to be made in order to test this assumption.

Additionally, the radon extraction results obtained in this work suggest that not all radon was extracted from the water. This could be improved by employing a higher helium flow and a longer extraction time. Regarding the extraction efficiency, additional studies have to be made as measurements hint on irregularities of the radon standard used to benchmark the procedure. To cross-check, the measurements should be repeated by enriching the water sample with a different radon source.

To conclude, despite the open questions mentioned above, the gas drying technique developed in this work was successfully integrated in the well established radon extraction procedure at MPIK. In order to be able to use the gas drying system for liquid samples in the future, the radon extraction efficiency from water has to be measured.

References

1. Bertone, G. & Hooper, D. A History of Dark Matter. arXiv: 1605.04909 (May 2016).
2. Undagoitia, T. M. & Rauch, L. Dark matter direct-detection experiments. arXiv: 1509.08767 (Sept. 2015).
3. Oort, J. H. H. The Force Exerted by the Stellar System in the Direction Perpendicular to the Galactic Plane and some Related Problems. *Bulletin Of The Astronomical Institutes Of The Netherlands* **6,** 249–287. ISSN: 0717-6163 (1932).
4. Garrett, K. & Duda, G. Dark Matter: A Primer. arXiv: 1006.2483 (June 2010).
5. Einasto, J. Dark Matter. arXiv: 1308.2534 (Aug. 2013).
6. Zwicky, F. Die Rotverschiebung von extragalaktischen Nebeln. *Helvetica Physica Acta* **6,** 110–127 (1933).
7. Bertone, G., Hooper, D. & Silk, J. Particle Dark Matter: Evidence, Candidates and Constraints. arXiv: 0404175 [hep-ph] (Apr. 2004).
8. Fixsen, D. J. The Temperature of the Cosmic Microwave Background. arXiv: 0911.1955 (Nov. 2009).
9. Planck Collaboration *et al.* Planck 2015 results. XIII. Cosmological parameters. arXiv: 1502.01589 (Feb. 2015).
10. *Particle Dark Matter* (ed Bertone, G.) ISBN: 9780511770739 (Cambridge University Press, Cambridge, 2010).
11. Selvi, M. Analysis of the seasonal modulation of the cosmic muon flux in the LVD detector during 2001-2008 . (2009).
12. The MACRO Collaboration & Ambrosio, M. Measurement of the residual energy of muons in the Gran Sasso underground Laboratories. *Astroparticle Physics* **19,** 313–328. ISSN: 09276505 (July 2002).
13. Aprile, E. *et al.* Dark Matter Search Results from a One Tonne$$Year Exposure of XENON1T. arXiv: 1805.12562 (May 2018).

14. XENON Collaboration *et al.* The XENON1T Dark Matter Experiment. arXiv: 1708.07051 (Aug. 2017).

15. Aprile, E. & Collaboration, X. The XENON1T Dark Matter Search Experiment. arXiv: 1206.6288 (June 2012).

16. The XENON collaboration *et al.* Physics reach of the XENON1T dark matter experiment. *Journal of Cosmology and Astroparticle Physics.* ISSN: 14757516. arXiv: 1512.07501 (Dec. 2015).

17. XENON100 Collaboration *et al.* Dark Matter Results from 100 Live Days of XENON100 Data. arXiv: 1104.2549 (Apr. 2011).

18. Aprile, E. *et al.* Conceptual design and simulation of a water Cherenkov muon veto for the XENON1T experiment. *Journal of Instrumentation* **9.** ISSN: 17480221. arXiv: 1406.2374 (June 2014).

19. Hagiwara, K. *et al.* Gamma Ray Spectrum from Thermal Neutron Capture on Gadolinium-157. arXiv: 1809.02664 (Sept. 2018).

20. Internal Communication.

21. Laubenstein, M. Messungen von 222Rn und 226Ra im Rahmen der Counting Test Facility des Sonnenneutrinoexperiments BOREXINO (1996).

22. Simgen, H. Messung von 222Rn und 226Ra in Wasser im Rahmen des Sonnenneutrinoexperiments BOREXINO (2000).

23. Wink, R. *et al.* The miniaturized proportional counter HD-2(Fe)/(Si) for the GALLEX solar neutrino experiment. *Nuclear Instruments and Methods in Physics Research Section A: Accelerators, Spectrometers, Detectors and Associated Equipment* **329,** 541–550. ISSN: 01689002 (June 1993).

24. Lindemann, S. Intrinsic 85Kr and 222Rn Backgrounds in the XENON Dark Matter Search, 184 (2013).

25. Wiesler, I. 222Rn-Emanationsmessungen im Rahmen des GERDA-Experiments (2006).

Erklärung

Ich versichere, dass ich diese Arbeit selbstständig verfasst und keine anderen als die angegebenen Quellen und Hilfsmittel benutzt habe.

Heidelberg, den 04.02.2019 .....

(Unterschrift)